Materials Today Bio 13 (2022) 100199

Contents lists available at ScienceDirect

Materials Today Bio

journal homepage: www.journals.elsevier.com/materials-today-bio

Engineering a naturally derived hemostatic sealant for sealing internal organs

Sevana Baghdasarian [a,1], Bahram Saleh [b,1], Avijit Baidya [a], Hanjun Kim [c], Mahsa Ghovvati [a], Ehsan Shirzaei Sani [a], Reihaneh Haghniaz [c], Shashank Madhu [b], Maria Kanelli [d], Iman Noshadi [e], Nasim Annabi [a,*]

[a] Department of Chemical and Biomolecular Engineering, University of California - Los Angeles, Los Angeles, CA, 90095, USA
[b] Department of Chemical Engineering Northeastern University, Boston, MA, 02115, USA
[c] Center for Minimally Invasive Therapeutics (C-MIT), California NanoSystems Institute (CNSI), University of California - Los Angeles, Los Angeles, CA, 90095, USA
[d] School of Chemical Engineering, National Technical University of Athens, Zografou Campus, Athens, 15780, Greece
[e] Department of Bioengineering, University of California, Riverside, 92507, USA

ARTICLE INFO

Keywords:
Hemostatic
Bioadhesive
Dopamine-conjugation
Double-crosslinked network
Photocrosslinking

ABSTRACT

Controlling bleeding from a raptured tissue, especially during the surgeries, is essentially important. Particularly for soft and dynamic internal organs where use of sutures, staples, or wires is limited, treatments with hemostatic adhesives have proven to be beneficial. However, major drawbacks with clinically used hemostats include lack of adhesion to wet tissue and poor mechanics. In view of these, herein, we engineered a double-crosslinked sealant which showed excellent hemostasis (comparable to existing commercial hemostat) without compromising its wet tissue adhesion. Mechanistically, the engineered hydrogel controlled the bleeding through its wound-sealing capability and inherent chemical activity. This mussel-inspired hemostatic adhesive hydrogel, named gelatin methacryloyl-catechol (GelMAC), contained covalently functionalized catechol and methacrylate moieties and showed excellent biocompatibility both *in vitro* and *in vivo*. Hemostatic property of GelMAC hydrogel was initially demonstrated with an *in vitro* blood clotting assay, which showed significantly reduced clotting time compared to the clinically used hemostat, Surgicel®. This was further assessed with an *in vivo* liver bleeding test in rats where GelMAC hydrogel closed the incision rapidly and initiated blood coagulation even faster than Surgicel®. The engineered GelMAC hydrogel-based seaalant with excellent hemostatic property and tissue adhesion can be utilized for controlling bleeding and sealing of soft internal organs.

1. Introduction

Centers for Disease Control and Prevention (CDC) have estimated that approximately 30 million surgical procedures are being performed annually in the United States [1]. Most of these procedures involve incisions from 1 to 2 cm in size in the case of minimally invasive surgeries, to 10–20 cm or greater in other cases. In general, these surgical wounds are always coupled with uncontrolled blood loss and can potentially facilitate chronicity and complications such as surgical site infection (SSI), prolonged hospitalization, increased cost, morbidity and mortality, and decreased quality of life. In addition, surgical wounds possess a greater risk for the patients suffering from host defense misfunctioning issues such as diabetes, autoimmune diseases, cancer, and others.

Traditionally, surgical wound closure procedures include the use of sutures, staples, or wires. However, using these techniques, particularly for parenchymatous tissues such as lung, liver, or kidney, can lead to necrosis and dehiscence of the wound. Apart from this, surgical procedures often trigger severe health complications related to hemorrhage. Even minimally invasive procedures face significant problems arising from the bleeding (e.g., compromising the vision during ocular procedure) [2]. Therefore, surgical sealants, with both hemostatic and wound sealing ability, have become a key component of the surgical toolbox to manage residual bleedings [3,4].

Today, in the era of sutureless surgical procedures, various protein-based (fibrin [5,6], collagen [7,8], gelatin [9,10]), polysaccharide-based (chitosan [11,12], and alginate [10]), and cyanoacrylate-based [13]

* Corresponding author.
E-mail address: nannabi@ucla.edu (N. Annabi).
[1] The authors Sevana Baghdasarian and Bahram Saleh made equal contribution to the work.

https://doi.org/10.1016/j.mtbio.2021.100199
Received 18 October 2021; Received in revised form 14 December 2021; Accepted 28 December 2021
Available online 29 December 2021

adhesives are utilized for various clinical wound closure applications [14,15]. While the primary focus of developing adhesive biomaterials is to reconnect damaged tissues and maintaining physiological activity, it could potentially stop bleeding from the injury sites by sealing. Meanwhile, cyanoacrylate-based synthetic glues with high adhesive and mechanical properties have exhibited considerable concerns related to their exothermic polymerization reaction, slow degradation rate, toxicity, and increased tissue inflammations [16,17]. Despite all the advantages of naturally derived polymer-based adhesives [18], weak tissue adhesion in wet physiological environments has shown significant concern towards their clinical use [19]. This is very important particularly for the treatment of wounds that are associated with bleeding, which make the environment wet in nature. Although a few adhesive hydrogels were developed that function well in the wet environments [10,20], their clinical applications are limited due to several issues. These include complex synthesis protocol, complicated application procedures, inability to control extensive bleeding, lack of elasticity, poor adhesion, and issues related to their biocompatibility and biodegradability [10,20–22]. Therefore, designing materials which can control bleeding while adhere to the wound is highly desired. Meanwhile, to explore the possibility of immediate clinical usage of such materials, tuning the chemistry of existing chemical functionalities could be beneficial.

To improve the adhesive properties of hydrogels to the wet tissue surfaces, mussel-inspired adhesion mechanism was utilized by incorporation of catechol moieties [23–28], which facilitates various chemical and physical interactions in the hydrogel-tissue interface [29]. For example, recently, a catechol-modified gelatin-based injectable hydrogel was introduced, which showed biocompatibility and considerable tissue adhesion [30]. However, the designed hydrogel showed poor mechanical strength due to the low crosslinking density. In another study, Kim et al. engineered a dopamine incorporated gelatin-based adhesive with high swellability [30]. In this case, the hydrogels exhibited low adhesion strength and dissolved within 24 h post-incubation period, reflecting lack of stability and inadequate cohesiveness. Meanwhile, catechol-incorporated bioadhesives have also been applied for antimicrobial and antifouling application, self-healing, drug delivery, and cancer treatment, etc [31,32]. Although several materials have been developed with catechol functionalities, designing a mechanically stable hemostatic sealant with improved adhesive characteristics can have significant clinical importance for immediate use.

Controlling bleeding from an injured tissue is a critical step in wound closure treatment [33]. These led to the use of different hemostatic agents such as fibrinogen and thrombin, and others which actively influence the blood coagulation cascade and accelerate the clot formation [2,34]. Many of these materials control hemostatic activity through their swelling characteristics [33]. Therefore, several hemostatic hydrogels were engineered with different coagulating agents to minimize the blood loss from the wound site [35]. For example, Kaolin-based QuikClot adhesive bandage [36] and gelatin-thrombin-based injectable Floseal [37] have already been introduced to market. Inorganic nanostructure (e.g., laponite) with a large negative surface charge, was also used to improve the hemostatic efficiency of the hydrogels [38–41]. Various naturally derived biopolymers such as chitosan, with polycationic structural backbone, enable nonspecific binding to cell membranes [34] and facilitate the coagulum formation in contact with whole blood. However, uncontrolled interaction of chitosan molecules with inflammatory cells has led to a strong foreign body response [42,43]. Meanwhile, due to lack of adhesive properties, oxidized cellulose-based commercially available hemostatic agents (e.g., Surgicel®), which easily control the bleeding and stimulate clotting, are only recommended to be used intraoperatively and removed after surgery [44]. Therefore, there is an unmet need to engineering a mechanically stable hemostatic sealant with improved wet adhesive properties for the treatment of injured/raptured internal organs that are especially associated with bleeding.

To address these limitations, herein, we have engineered a multifunctional hydrogel that showed improved *in vitro* and *in vivo* hemostatic activity without compromising the adhesion performance to the wet biological surfaces. The hydrogel, named gelatin methacryloyl-catechol (GelMAC), was synthesized with a chemically modified gelatin backbone which was covalently conjugated with biologically inspired catechol motifs and photocrosslinkable methacrylate groups. The designed hydrogel contained double-crosslinked 3D networks through Fe^{3+} ion mediated chelation and visible-light induced covalent interactions. The physical properties of the synthesized hemostatic sealant was characterized including mechanical properties, swelling ratio, degradability, and adhesion. In addition, the biocompatibility of GelMAC hydrogels was evaluated through both *in vitro* and *in vivo* studies, using fibroblast cells and a rat subcutaneous model. Finally, the *in vivo* hemostatic property of GelMAC hydrogel was demonstrated in a rat liver bleeding model and compared with clinically used hemostatic materials to highlight the potential of engineered hydrogel for clinical uses.

2. Experimental section

2.1. Materials

Gelatin from porcine skin, methacrylic anhydride (MA), dopamine hydrochloride, (Benzotriazol-1-yloxy)tris(dimethylamino)phosphonium hexafluorophosphate (BOP), 1-Hydroxybenzotriazole hydrate (HOBt), Eosin Y disodium salt, Triethanolamine (TEA), N-Vinylcaprolactam (VC), hematoxylin-eosin y staining (H&E) solutions, Iron(III) chloride, and 3-(Trimethoxysilyl)propyl methacrylate (TMSPMA) were purchased from Sigma-Aldrich. Collagenase type II was purchased from Worthington Biochemical Co. Dulbecco's modified Eagle medium (DMEM) was purchased from Cellgro (Manassas, VA), Fetal Bovine Serum (FBS) and Dulbecco's phosphate-buffered saline (DPBS) were obtained from HyClone (Logan, UT). Live/Dead viability kit, and penicillin/streptomycin (Pen-Strep) were purchased from Invitrogen (San Diego, CA), and fresh human whole blood was purchased from ZenBio.

2.2. Synthesis of GelMA

GelMA was synthesized as described previously [45,46]. Briefly, gelatin from porcine skin (10 g) was dissolved in 100 ml Dulbecco's phosphate-buffered saline (DPBS) at 50 °C. A 8% (v/v) methacrylic anhydride (MA) solution was added dropwise under continuous stirring at 50 °C. After 3 h, the solution was diluted with 200 ml DPBS to stop the reaction. The diluted solution was dialyzed against deionized (DI) water at 50 °C for 5 days. The resulting solution was then filtered under sterile conditions, frozen at −80 °C overnight, and lyophilized for 5 days.

2.3. Synthesis of GelMAC

First 800 ml of deionized (DI) water was bobbled with nitrogen gas for 30 min to remove air from the DI water. Then, 2 g of gelatin from porcine skin was added at a final concentration of 2.5 mg/ml to water at 50 °C. Next, 517.1 mg (~3.41 mM) of dopamine hydrochloride was dissolved in 3ml of DI water, and 353.8 mg (~1.00 mM) of BOP ((benzotriazol-1-yloxy) tris(dimethylamino)phosphonium hexafluorophosphate) and 122.5 mg (~1.13 mM) of HOBt (1-hydroxybenzotriazole) were dissolved in 3 ml of Dimethylsulfoxide (DMSO) and injected into the reaction mixture. Then, 1339 μl (~12 mM) of triethylamine was injected into the reaction mixture. The reaction mixture was continuously stirred with a stir bar for 2 h under N_2 atmosphere. The reaction mixture was closely observed to ensure achievement of a clear and color less mixture during this 2 h. Chemically modified gelatin with dopamine was precipitated with excess cold acetone (~1.2 L) and then re-dispersed in 100 ml of DPBS to be metacrylated utilizing MA as previously described [45,46]. Briefly, gelatin was dissolved in DPBS at a concentration of 2% (w/v) and heated and bubbled with nitrogen gas at 50 °C for 30 min. Next, 8% (v/v) MA was added to the reaction mixture dropwise under continuous stirring at 50 °C. This step was followed by diluting the reaction mixture after 2 h with DPBS. Finally, the

solution was dialysis against DI water at 40–50 °C for 5 days. After sterile filtration and lyophilization for 5 days, GelMAC prepolymer was stored at 4 °C until experimental use.

2.4. Chemical characterization of GelMAC

Chemical functionalization of gelatin molecule was confirmed with proton nuclear magnetic resonance (^{1}H NMR) spectroscopy analysis using a 400 MHz Bruker AV400 spectrometer. To calculate the degree of conjugation, recorded spectra were corrected with phase and base line and solvent peak. The samples were prepared by dissolving 5–10 mg of the dried polymers in 1 ml of DMSO-d_6. Herein, peak at 7.2 ppm was used as a refence and the change in -CH_2 peak at 2.75 was integrated to calculate the degree of conjugation. Meanwhile, change in the peak at δ = 5.6 ppm related to methacrylate group was integrated to calculate the degree of crosslinking. For the Fourier-transform infrared spectroscopy (FTIR) analysis, 2–5 mg of samples were grinded with dry KBr to make palette and further used for the measurements in a PerkinElmer Paragon 1000 FT-IR Spectrometer.

2.5. Hydrogel preparation

The lyophilized GelMAC and GelMA prepolymers was first dissolved in a solution containing Triethanolamine (TEA) and N-Vinylcaprolactam (VC) in DPBS. Iron chloride solution at various iron concentrations (0, 1, 2.5, 5 mM) was prepared and stored in 4 °C prior to use. Eosin Y disodium salt was dissolved separately in DPBS and was then added to the prepolymer/TEA/VC solution to form the hydrogel precursor. Finally, Fe^{+3} at desired concentration was added to the mixture. The final concentration of each component in the mixture is as follows: 20% prepolymer, 1.875% (w/v) TEA, 1.25% (w/v) VC, 0.1 mM Eosin Y, and various concentrations of Fe^{+3}(0, 1, 2.5, 5 mM). To form the hydrogels, the prepolymer solution was injected at the desired surface and immediately photocrosslinked for 4 min, using a LS1000 FocalSeal Xenon Light Source (Genzyme).

2.6. Mechanical properties

The prepolymer solution was prepared as described above. A 70 μl volume of the prepolymer solution was pipetted into a polydimethylsiloxane (PDMS) cylindrical mold (diameter: 6 mm; height: 2.5 mm). The solution was then photopolymerized via exposure to visible light (450–520 nm) for 4 min. The precise dimension of each sample was measured using a digital caliper. Each sample was then carefully placed on the compression plate of an Instron 5943 mechanical tester. The test was conducted at a rate of 1 mm/min up to a maximum strain of 70%. The load and compressive strain values were recorded utilizing a Bluehill® 3 software. The Young's modulus was calculated from the slope of the linear region in the stress-strain curve [47].

2.7. In vitro swelling ratio

The swellability of GelMAC and GelMA hydrogels was defined by calculating the ratio of weight change at each time point to the initial weight of the hydrogel after inclubation in DPBS at 37 °C. For this, hydrogels were formed as described in the previous section and weighed (initial weight) following by submerging them into DPBS at 37 °C. Excess buffer was gently removed using a disposable wipe, and the wet weight of the hydrogels was measured at different time points for up to 48 h.

2.8. In vitro enzymatic degradation

To evaluate the percentage of *in vitro* degradation, GelMAC and GelMA hydrogels were weighed immediately after crosslinking, and placed in separate wells of a 24 well plate. Each well was then filled with 1 ml of DPBS containing 20 μg/ml collagenase type II [48] and kept at 37 °C. The enzyme-containing DPBS solutions were changed every 2 days during the entire duration of this experiment. The samples were then freeze-dried and weighed on days 1, 4, 7, 10, 12, 14, 16, 20, and 22 post-incubation. The percentage degradation of the gels was determined using Eq. (1).

$$Degradation(\%) = \frac{W_0 - W_t}{W_0} \times 100 \quad (1)$$

where W_o is the initial sample dry weight, and W_t is the dry weight after time t.

2.9. In vitro wound closure

The adhesion strength of the GelMAC and GelMA hydrogels was evaluated according to a modified ASTM testing methodology (ASTM F2458-05). Briefly, a fresh porcine lung was obtained from a local slaughterhouse and was cut into rectangular sections (10 mm × 40 mm). The porcine lung was kept moist with DPBS prior to use. The tissues were fixed onto two precut glass slides (30 mm × 40 mm) using Krazy Glue. The tissue was then cut from the middle with a single edge cutter blade. Next, 50 μl of the precursor solution was pipetted onto the tissue interface covering a total surface area of 10 mm × 10 mm enclosed by each tissue ends and subsequently crosslinked with visible light for 4 min. Upon placing the samples between the tensile grips of an Instron mechanical tester, the ultimate adhesive strength was measured at failure point.

2.10. In vitro burst pressure

The burst pressure of the GelMAC and GelMA hydrogels were measured based on the standard ASTM F2392-04 testing methodology. The porcine intestine tissue was first cut to a dimension of 40 mm × 40 mm and rehydrated using PBS. Next, the tissue was placed between two stainless steel plates (35 mm × 35 mm), in which the upper plate had a 10-mm-diameter opening located at its center. A circular defect (2 mm in diameter) was then created at the center of the tissue assembled in between the two metallic plates. A 20 μl of the prepolymer solution was injected over the defect site and exposed to visible light. Next, using a syringe pump (Syringe Pump NE-1000) air was continuously pumped into the system at a rate of 10 ml/min while the pressure inside the system was measured using a PASCO wireless pressure sensor. The system was pressurized until a burst was observed through the escape of bubbles from the defect site.

2.11. Cell viability and proliferation assays

The NIH 3T3 fibroblasts were mixed with the hydrogel precursor, and a 12 μL drop of it was placed in a spacer with 150 μm height and covered by a 3-(trimethoxysilyl) propyl methacrylate (TMSPMA) coated glass (2 × 10^5 cells/samples). Then, the hydrogel precursor was photopolymerized for 20 s using visible light, and the samples were placed in 24-well plates with 1 ml of growth medium (DMEM + 10% FBS+ 1% Pen-Strep). 3D cultures were incubated at 37 °C in a 5% CO_2 humidified atmosphere for 7 days, and the growth medium was replaced every 2 days. Cell viability was determined using a calcein AM/ethidium homodimer-1 live/dead kit (Invitrogen) following the manufacturer's instructions. The viability of 3D encapsulated NIH 3T3 fibroblasts in GelMAC-Fe were evaluated on days 1, 4, and 7 post-encapsulation. Fluorescent images were taken using a Zeiss Axio Observer Z1 inverted microscope and were analyzed with the ImageJ software. Cell viability was calculated as the ratio of viable cells to the total number of live and dead cells. The PrestoBlue assay was utilized to evaluate the metabolic activity of 3D encapsulated NIH 3T3 fibroblasts inside the GelMAC-Fe hydrogels on days 1, 4, and 7 post-incubation. The fluorescence intensity of the resulting solutions was recorded at 535–560 nm excitation and 590–615 nm emission.

2.12. In vitro blood clotting assay

Blood clotting study on hydrogels was performed in the presence of recalcified blood following a published protocol [41]. Briefly, a volume of 630 μL fresh blood in addition with the anticoagulant sodium citrate (ASC) (9:1) was pipetted into a 1.5 ml Eppendorf tube. A total of 70 μL of 0.1 M calcium chloride ($CaCl_2$) was then added, followed by vortexing for 10 sec. Then, 100 μL was deposited into sequential wells of a 48 well plate. At selected time points, each well was washed with 9 g/L saline solution to halt clotting. The liquid was immediately aspirated, and washes were repeated until the solution was clear, indicating the removal of all soluble blood components. In case of the GelMAC and GelMA experimental groups, the prepolymer solutions were pipetted at the base of the well plates, ensuring the entire bottom surface was coated with the hydrogel and photocrosslinked in advance. After a trial was complete, the final clotting time was marked in the well that formed a uniform clot, with no change in clot size in the subsequent wells.

2.13. In vitro blood compatibility test and hemolysis ratio measurement

In vitro blood compatibility study on hydrogels was performed as described in a previously published article [48]. Briefly, the crosslinked hydrogels were rinsed three times with DI water and DPBS before being placed into 15 ml falcon tubes. Then, 10 ml DPBS was added into the tubes and kept at 37 °C on a shaker incubator for 3 h. In the next step, 4 ml of ASC-whole blood was first diluted with 5 ml DPBS and 0.2 ml of this solution was dropped into the tubes allowing the hydrogels to be soaked in the blood solution for 1 h. Next, the solutions were aspirated and centrifuged at 100×*g* for 10 min and the absorbance of the supernatants was measured at 542 nm by using a spectrophotometer. The hemolysis ratio (HR) was obtained by using the following equation

$$HR = (AS - AN)/(AP - AN) \quad (2)$$

Where AS is the absorbance of the sample supernatant, and AN and AP are the absorbance of the negative control (10 ml DPBS + 0.2 ml diluted ASC-whole blood), and the positive control (10 ml pure water + 0.2 ml diluted ASC-whole blood), respectively.

2.14. Subcutaneous implantation in rats

All animal experiments were reviewed and approved by Institutional Animal Care and Use Committee (ICAUC; protocol15e1248R) at Northeastern University (Boston, MA, USA). Male Wistar rats (200–250 g) were obtained from Charles River (Boston MA, USA) and housed in the local animal care facility under conditions of circadian day-night rhythm and feeding ad libitum. Anesthesia was achieved by isoflurane (2.5%) inhalation, followed by the administration of SC buprenorphine (0.02–0.05 mg/kg). After inducing anesthesia, eight 1-cm incisions were made on the posterior dorsomedial skin, and small lateral subcutaneous pockets were prepared by blunt dissection. Sterile, lyophilized, and pre-weighted cylindrical-shaped GelMA-Fe and GelMAC-Fe hydrogels samples were implanted in subcutaneous pockets along the dorsomedial skin of male Wistar rats. At days 7, 28, and 56 post-implantation, animals were euthanized, and the hydrogels were retrieved along with the surrounding tissues for histological assessment and were immediately placed in a 4% paraformaldehyde solution. Hydrogel samples used for biodegradation studies were immediately weighted, lyophilized, and re-weighted.

2.15. Liver bleeding tests in rats

All animal experiments were approved by the UCLA Animal Research Committee (UCLA ARC #2017-096-01) and coducted in accordance with the relevant guidelines. The animals were weighed and monitored daily for signs of pain or discomfort during the experimental period. A set of 6 experimental groups were selected for this study which included the no treatment group (injury only) as the negative control, the GelMA hydrogel with or without Fe^{3+} ions, the GelMAC hydrogel with or without Fe^{3+} ions, and the commercial absorbable hemostatic agent, Surgicel® (Ethicon, Cincinnati, OH, USA) to serve as positive control group. Under general anesthesia (1.5% isoflurane in 100% O_2), median laparotomy was conducted, a wound retractor was placed, and the operating field around the liver was draped with filter paper to collect the entire amount of blood loss from the incision site. A standardized liver wound was made using a 2 mm-sized biopsy punch. Immediately, the sterile hydrogel prepolymer solution was applied to the bleeding lesion and crosslinked for 4 min with visible light. The amount of blood absorbed by the filter paper was immediately measured and recorded. Afterward, the abdominal wound was anatomically closed using 4–0 absorbable sutures and 4–0 non-absorbable sutures/staples by closing the peritoneum and the abdominal skin separately. The relative bleeding amount was calculated using Eq. (3).

$$\%\ \text{Relative Bleeding Amount} = \frac{\text{Weight of the collected blood}}{\text{Average weight of the collected blood in the injury only group}} \times 100 \quad (3)$$

2.16. Morphological assessment and histopathological evaluation

Hydrogel samples along with surrounding tissue regions were explanted and used for histopathological analysis (8-μm cryosection slides). The extracted hydrogel-tissue samples were incubated with 30% sucrose solution overnight, followed by overnight incubation in 100% FBS. Next, they were flash-frozen in liquid nitrogen in Optimal Cutting Temperature (OCT) Compound. 8-μm cryosections were acquired using a Leica Biosystems CM3050 S Research Cryostat and processed with H&E staining.

2.17. Data analysis

Data analysis was carried out using a 1- or 2-way ANOVA test with GraphPad Prism 6.0 software. Error bars represent mean ± standard deviation (SD) of measurements (*$p < 0.05$, **$p < 0.01$, ***$p < 0.001$, and ****$p < 0.0001$).

3. Results and discussions

3.1. Synthesis and chemical characterization of GelMAC hemostatic sealant

The chemical synthesis of gelatin methacryloyl-catechol (GelMAC) and its application over injured tissue surface is schematically represented in Fig. 1A. Here, the use of naturally derived gelatin biopolymer with hydroxyl (-OH), amine (NH_2), and carboxylic acid (COOH) groups facilitated the chemical conjugation of biologically inspired catechol motifs and photocrosslinkable methacrylate groups (Fig. S1). In addition, it is also known that gelatin-based hydrogels provide biocompatibility and biodegradability which are important for tissue engineering applications [45]. During the synthesis, in the first step, dopamine molecules were covalently linked with carboxylic acid groups through the formation of amide bonds [49]. After that, the methacrylate group was chemically functionalized with amine (NH_2) and hydroxyl (-OH) residues

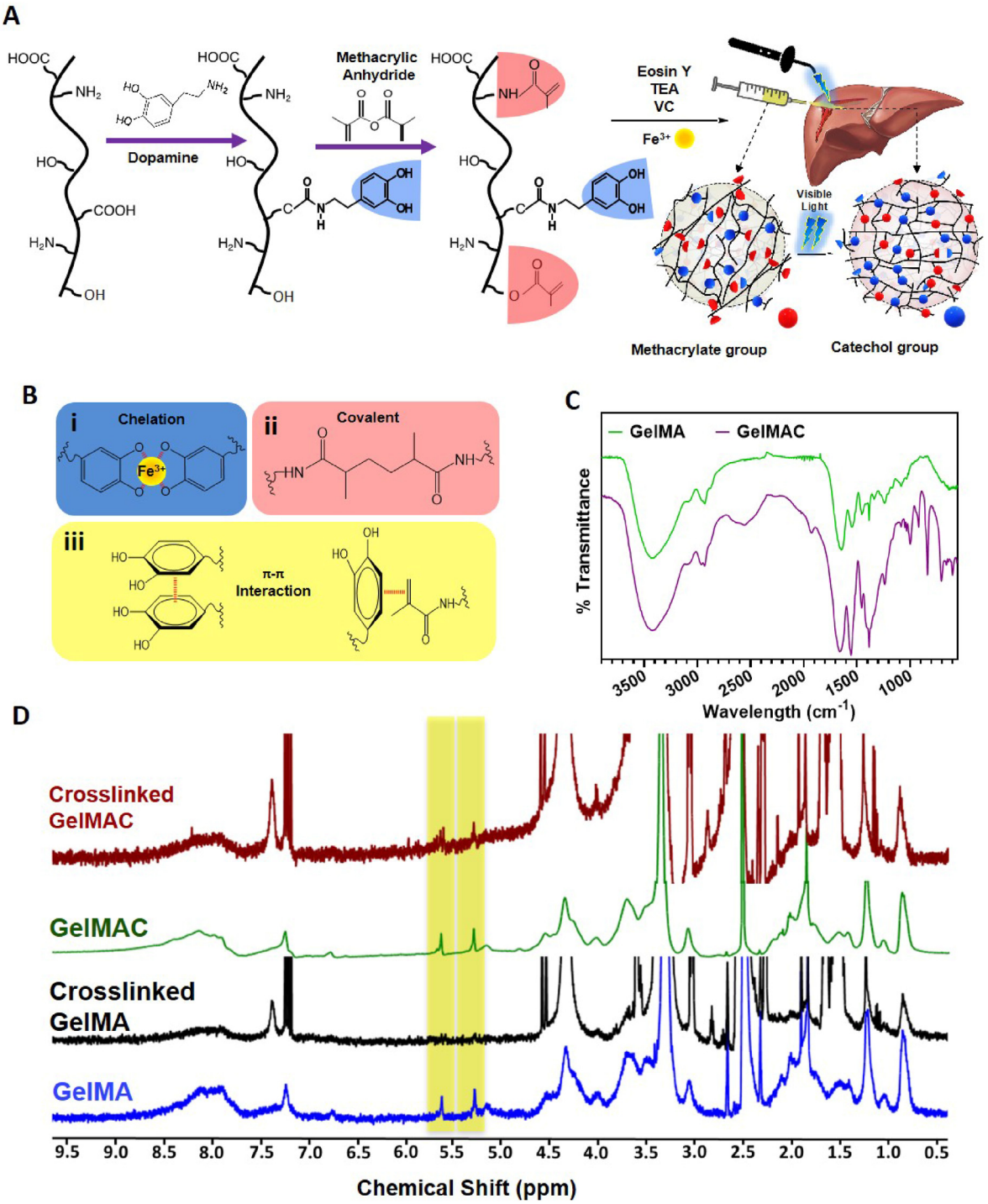

Fig. 1. Synthesis and chemical characterization of GelMAC prepolymer. A) Schematic illustration for the synthesis of GelMAC and its application as a hemostatic sealant. **B)** Covalent and non-covalent interaction in GelMAC hydrogel. **(i)** Fe^{3+}ion mediated chelation, **(ii)** C-C covalent bond formation between methacrylate groups upon photocrosslinking, and **(iii)** π-π interactions between aromatic moieties of chemically conjugated dopamine molecules. **C)** Representative FTIR spectra of GelMA and GelMAC prepolymers. **D)** ^{1}H NMR spectra of GelMA and GelMAC before and after crosslinking.

of the gelatin backbone [10,46] (Figs. 1A and S1). To fabricate the GelMAC hydrogel, along with mixing with Fe^{3+} ions, prepolymer solution was further irradiated with visible light. The visible-light-initiated photocrosslinking, using Eosin Y as a photoinitiator, Triethanolamine (TEA) as a co-initiator and N-vinylcaprolactam (VC) as a co-monomer has been explained thoroughly before [50]. While photocrosslinking reaction facilitated the formation of C-C covalent bond between the MA groups [10,49], Fe^{3+} ions introduced non-covalent interactions between the catechol groups through chelation mechanism (Fig. 1B–i,ii) [31]. Chemically, these covalent interactions (C-C) contributed to the primary structure of the GelMAC hydrogel. The catechol-induced non-covalent functional interactions [31,51] in the GelMAC hydrogel is also shown in Fig. 1B–iii. Eventually, incorporation of such sequential inter and intramolecular covalent and non-covalent interactions led to the formation of a double-crosslinked hydrogel network.

Chemical conjugation of dopamine molecules was confirmed with Fourier-transform infrared spectroscopy (FTIR). Fig. 1C represents the FTIR spectra of GelMAC and GelMA. Peak around 1000 cm^{-1} in GelMAC

spectrum, which corresponds to aromatic C-H bending of catechol moieties, proved the presence of dopamine molecules in gelatin backbone [52,53]. This was further confirmed with the peak at 1550 cm^{-1} related to aromatic C-C stretching of dopamine moieties [53]. Meanwhile, the appearance of vinyl C-H peaks in proton nuclear magnetic resonance (^{1}H NMR) spectra of GelMA and GelMAC at $\delta = 5.3$ and 5.6 ppm (Fig. 1D, marked in yellow), respectively, confirmed the covalent linkage of methacrylate groups with gelatin biomacromolecules. Multiple peaks in the region of 6.5 ppm in ^{1}H NMR spectrum of GelMAC could be related to the catechol moieties which was not seen for GelMA (Fig. S2). The degree of the conjugation of methacrylate groups in GelMA and GelMAC polymers was calculated from the ^{1}H NMR spectra [45] and observed to be ~55% and ~50%, respectively. This difference could be attributed to molecular steric hindrance due to the presence of covalently linked dopamine molecules on GelMAC polymers [54–56]. Meanwhile, the degree of crosslinking for both GelMA and GelMAC were calculated with ^{1}H NMR spectra of crosslinked and uncrosslinked hydrogels as presented in Fig. 1D. While the degree of crosslinking for GelMA hydrogel was observed to be over 90%, GelMAC, containing dopamine moieties, exhibited a reduced degree of crosslinking in the range of 65%. This could be attributed to the radical scavenging characteristic of dopamine moieties with an aromatic ring, which hindered the photopolymerization [57–60]. Moreover, GelMAC prepolymer solution was found to exhibit higher viscosity compared to the GelMA as shown in Fig. S3. This might be associated with the existence of catechol moieties that form intra and inter molecular π- π interactions.

3.2. Physical characterization of GelMAC hemostatic sealant

For a soft hydrogel to be used as a hemostatic sealant, a balance between mechancial properties (cohesion), and adhesion is required [34]. Based on Fig. 2A, the Young's modulus of GelMAC hydrogel formed using various Fe^{3+} ion concentrations in compression test were lower than respective GelMA hydrogels. This decreased mechanical stiffness in GelMAC hydrogels compared to GelMA could be due to the lower degree of crosslinking in GelMAC system as confirmed by ^{1}H NMR analysis in Fig. 1D. Meanwhile, both GelMAC and GelMA hydrogels formed with 2.5 mM Fe^{3+} ion concentration showed a significant increase in Young's modulus as compared to GelMAC and GelMA hydrogels engineered without Fe^{3+} (Fig. 2A). For example, the Young's modulus for GelMAC hydrogels without and with Fe^{3+} (2.5 mM) were 172.5 ± 9.2 and 260.2 ± 19.4 kPa, respectively. Similarly, the Young's modulus for GelMA hydrogels without and with (2.5 mM) Fe^{3+} were 275.2 ± 40.5 and 377.9 ± 60 kPa, respectively. Such improvement could be related to non-covalent interactions of Fe^{3+} ions with gelatin backbone in both GelMAC and GelMA networks [61]. In addition, particularly for GelMAC hydrogel with catechol moieties, Fe^{3+} ions could easily form a secondary network through noncovalent chelation interactions that could contribute towards improved mechanics [62–65]. The obtained stiffness for GelMAC hydrogel was significantly higher than UV light crosslinked GelMA-DOPA hydrogel (120 ± 12 kPa) reported by Cheng et al. [66]. Meanwhile, the Young's modulus of GelMAC and GelMA hydrogels were not changed significantly upon further increase in Fe^{3+} ions concentration from 2.5 to 5 mM, which could be due to the saturation in ionic interactions between Fe^{3+} ions and gelatin backbone.

The adhesive property of GelMAC hydrogel was studied by using a standard wound closure test where pig lung tissue was used as the biological substrate (Fig. 2B). For GelMAC and GelMA hydrogels without Fe^{3+}, the adhesive strength was 33 ± 3.2 kPa and 19.2 ± 1.4 kPa, respectively. Similarly, GelMAC and GelMA hydrogels formed with 2.5 mM Fe^{+3} ion concentration exhibited the adhesive strength of 33.7 ± 3.8 and 22 ± 1.32 kPa, respectively. The increased adhesive strength for GelMAC hydrogel as compared to GelMA could be due to the presence of the catechol moieties in the hydrogel backbone [31]. To be used as a surgical hemostatic sealant, the adhesive performance of the GelMAC hydrogels were compared with clinically used bioadhesives and hemostatic materials (Fig. 2B), including Coseal® (sealant, polyethylene glycol-based), Evicel® (hemostatic sealant, human fibrin-based), and Surgicel® (hemostat, oxidized cellulose-based). The adhesion strength of GelMAC hydrogel formed with 2.5 mM Fe^{3+} ion concentration was comparable with the adhesion strength of clinically used surgical sealant, Coseal® (Fig. 2B). Meanwhile, all the hydrogel compositions, including GelMAC-based hydrogels, formed with 2.5 mM Fe^{3+} ion concentration, showed significantly improved adhesion capability compared to both hemostatic materials, Evicel® and Surgicel® (Fig. 2B). This increase could be due to the interfacial interactions between GelMAC hydrogel and tissue surfaces as presented in Fig. 3C. These include both covalent and non-covalent interactions formed due to photocrosslinking, and the presence of catechol moieties and other functional groups present in GelMAC backbone [10,31]. Therefore, the engineered hydrogel with excellent adhesive characteristic and improved mechanical stability can potentially be used clinically for sealing and controlling hemorrhage from a raptured tissue or incision during the surgeries.

The adhesive properties of the engineered GelMAC hydrogel were further characterized with a standard ASTM burst pressure test (Fig. S4). The pressure values for both GelMAC and GelMA hydrogels formed by using various concentrations of Fe^{3+} ions were measured. As shown in Fig. S4, burst pressure for GelMAC hydrogels containing 5 mM Fe^{3+} ions (44.8 ± 3.1 kPa) was significantly higher than the GelMA hydrogels formed with 5 mM Fe^{3+} ions (21.2 ± 4.8 kPa), confirming the contribution of catechol groups in improving the adhesion strength of the resulting bioadhesives.

Ability to absorb water is another characteristics of material that can control hemostasis [67]. *In vitro* swellability of the engineered GelMAC hydrogels was tested at 37 °C for 48 h. GelMAC hydrogels, formed with different concentrations of Fe^{3+} ions, reached maximum swelling at a longer time as compared to the GelMA hydrogels formed with the same Fe^{3+} ion concentration (Figs. 2D and S5A). For example, the maximum swelling for GelMA and GelMAC hydrogels, formed with different concentrations of Fe^{3+} ions, was achieved within 1 h and 4 h, respectively. This could be related to the additional interactions in GelMAC network due to the presence of catechol moieties in its backbone. Meanwhile, the higher swelling ratio for GelMAC hydrogels, formed with 2.5 mM Fe^{3+} ion concentration, as compared to GelMA hydrogels (Fig. 2E) were due to the lower degree of crosslinking in GelMAC network which enabled water molecules to diffuse easily inside the hydrogel matrix. In addition, GelMAC hydrogel contained hydrophilic catechol functionalities, which might also influence the swelling ratio of the resulting hydrogel. To demonstrate the biodegradability of GelMAC hydrogels, *in vitro* enzymatic degradation was performed in DPBS containing collagenase type II (20 μg/ml) over 21 days. Although, GelMAC hydrogels had lower degree of covalent crosslinking through photopolymerization, both GelMAC and GelMA hydrogels, formed with different Fe^{3+} ion concentrations, showed similar degradation pattern (Fig. 2F,G and S5B). This could be related to the effect of dual crosslinking in GelMAC hydrogel formed with catechol-Fe^{3+} interactions.

3.3. In vitro clotting time and blood compatibility of GelMAC hemostatic sealant

Controlling bleeding from the wound site, especially during surgery, is highly desired. In this context, different hemostatic materials are widely used in various clinical settings and combat environments [3,33]. These materials mostly control absorption of blood fluid and coagulation mechanism with the clotting factors [33,67]. Surgicel® is an example of commercially available hemostatic material which is known to perform better than other commercial materials and widely used in clinical practice [4,68]. Meanwhile, to control the bleeding, hemostatic sealants were also developed which offered both tissue sealing and hemostasis. For example, Wang and coworkers recently developed tetra-poly(ethylene glycol) based composite hydrogel that showed wet adhesion and hemostatic capability at the same time [69]. Similarly,

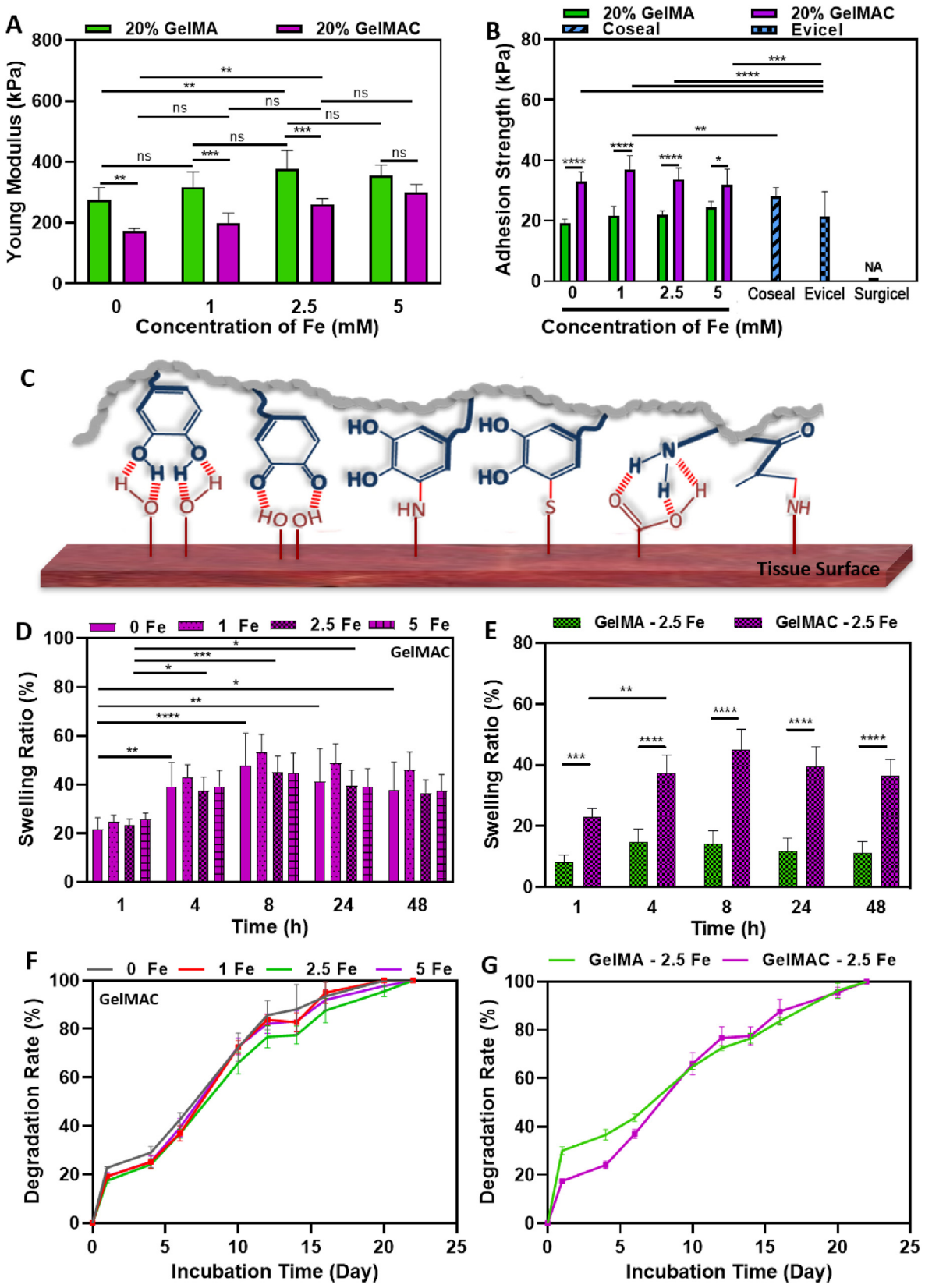

Fig. 2. Physical characteristics of GelMAC and GelMA hydrogels. **A)** Young modulus of hydrogels containing various Fe^{3+} ion concentrations based on compression test, **B)** *In vitro* adhesion strength of hydrogels containing various Fe^{3+} ion concentrations compared with Coseal®, Evicel®, and Surgicel® using porcine lung tissue. **C)** Schematic representation of functional interactions at GelMAC hydrogel-tissue interface. **D)** Swelling ratio of GelMAC hydrogels containing various concentrations of Fe^{3+} ion in DPBS **E)** Swelling ratio of GelMA and GelMAC hydrogels containing 2.5 mM Fe^{3+} ion concentration in DPBS, **F)** Degradation rate of GelMAC hydrogels containing various concentrations of Fe^{3+} ion in enzyme-containing DPBS solution, **G)** Degradation rate of GelMA and GelMAC hydrogels containing 2.5 mM Fe^{3+} ion concentration in enzyme-containing DPBS solution. Data are represented as mean ± SD (*$p < 0.05$, **$p < 0.01$, ***$p < 0.001$ and ****$p < 0.0001$, $n \geq 6$).

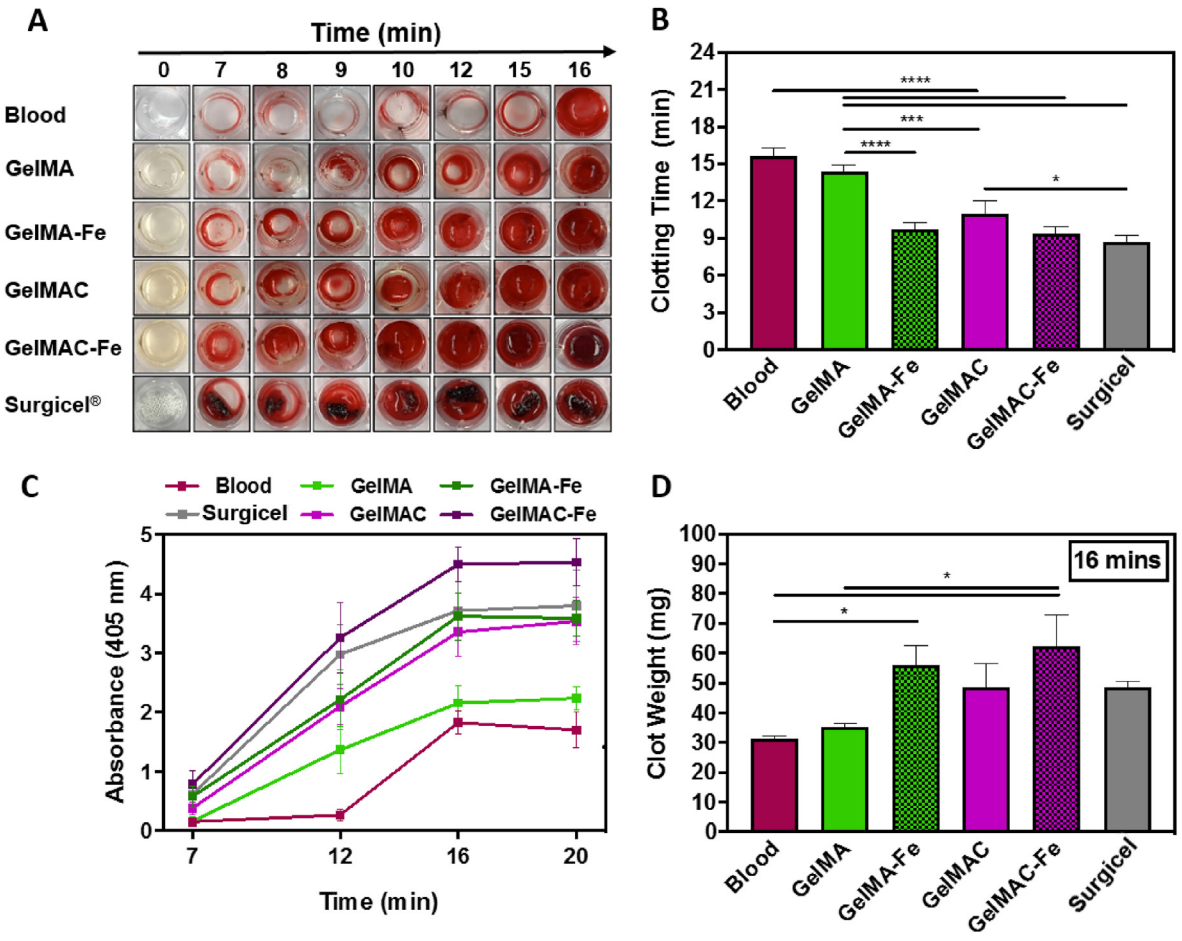

Fig. 3. *In vitro* hemostatic properties of the of GelMAC and GelMA hydrogels. A) Time-dependent clot formation of GelMA, GelMAC, GelMA-Fe, and GelMAC-Fe hydrogels compared with untreated blood (negative control) and Surgicel® absorbable hemostatic gauze (positive control), **B)** Quantitative clot formation time, **C)** Absorbance at 405 nm wavelength performed on clotted samples at various time points of 7, 12, 16, and 20 min. **D)** Clot weight collected at 16 min time point. Data are represented as mean ± SD (*$p < 0.05$, ***$p < 0.001$, ****$p < 0.0001$ and $n = 4$).

Ouyang et al. designed extracellular matrix mimicked GelMA-based adhesive hydrogel that rapidly adhered and sealed bleeding arteries and cardiac walls upon UV light irradiation [35]. However, clinical utility of these materials are limited due to long gelling time, poor mechanical properties, and low biocompatibility [20,69,70]. Therefore, engineering tissue adhesives with hemostasis ability similar to Surgicel® is beneficial. Herein, GelMAC and GelMA hydrogels, formed with 2.5 mM Fe^{3+} ion, were chosen and tested for hemostasis due to their improved mechanics and adhesion properties as compared to the others hydrogel formed with different Fe^{3+} ion concentration. Superior hemostatic ability of GelMAC hydrogel (with and without Fe^{3+}) as compared to GelMA (with and without Fe^{3+}), and most widely clinically used hemostatic material, Surgicel® is demonstrated in Fig. 3A. Meanwhile, blood clotting times were calculated for 6 test groups including whole blood (negative control), GelMA, GelMA-Fe, GelMAC, GelMAC-Fe, and Surgicel® and presented in Fig. 3B. The GelMAC hydrogel significantly reduced the blood clotting time to 11 ± 1 min, compared to the GelMA hydrogels (with blood clotting time of 14.3 ± 0.6 min) which is similar to the clotting time for untreated blood (15.6 ± 0.3 min). In this case, along with the catechol moieties on the GelMAC backbone that facilitated the interactions with serum proteins and other blood cells (e.g., erythrocytes, white blood cells, or platelets), higher swelling of GelMAC (Fig. 2E) played an important role for blood coagulation [71,72]. Whereas lower swelling ratio of crosslinked GelMA could limit the hemostatic ability of hydrogel. Chemically, Fe^{3+} ions readily interact with blood proteins through the extended electrostatic and hydrogen bonding interactions [73]. Therefore, incorporation of Fe^{3+} ions in both GelMAC and GelMA hydrogels further decreased the blood clotting time to 9.3 ± 0.6 and 9.7 ± 0.6 min, respectively. Effect of Fe^{3+} ions in blood coagulation [74] was clearly observed in case of GelMA-Fe where unbound Fe^{3+} ions in hydrogel structure could easily diffuse and contribute towards hemostatic activity. Thus, GelMAC-Fe hydrogel showed dual functionality (adhesion and hemostatic), which is required for the treatment of bleeding wounds. Blood clotting efficiency for both GelMAC-Fe and GelMA-Fe were comparable to Surgicel® (with blood coagulation time of 8.7 ± 0.6 min), which lacked any kind of tissue adhesion (Fig. 2B). Enhanced hemostatic activities of the engineered bioadhesives were further characterized with absorbance and clot weight measurements. To further evaluate the coagulation process, UV-visible absorbance at 405 nm [75] was measured at different time points (at 7, 12, 16, and 20 min) and presented in Fig. 3C. No significant change in absorbance after 16 min confirmed the completion of the blood coagulation process. Meanwhile, higher absorbance values for GelMAC-Fe hydrogel compared to Surgicel®, confirmed its enhanced hemostatic activity. In addition, weight of the collected blood clot associated with GelMAC-Fe hydrogel at 16 min time point was observed to be higher than GelMA hydrogel, GelMA-Fe hydrogel, and Surgicel® (Figs. 4D and S6). These data collectively highlighted the *in vitro* hemostatic efficacy of GelMAC-Fe hydrogel for wound management.

We also evaluated blood compatibility of the hydrogels *in vitro* by measuring HR values, which indicate the extent of red blood cells (RBC) broken by the hydrogels in contact with blood. A smaller HR value translates into increased blood compatibility of biomaterials (indicating small amount of broken RBC) [48]. In addition, it is known that the HR

values of biomaterials should be below 5 for medical applications [76]. As shown in Fig. S7, the HR values for all tested hydrogels (GelMA, GelMA-Fe, GelMAC, and GelMAC-Fe) was less than 0.25, confirming their blood compatibility.

3.4. *In vitro and in vivo biocompatibility of GelMAC hemostatic sealant*

For designing a surgical sealant, biocompatibility of the material is considered as one of the most important parameters. Therefore, cytocompatibility of GelMAC-Fe and GelMAC-Fe hydrogels (20% (w/v)) were studied both *in vitro* and *in vivo* to ensure that there was no toxicity due to the introduction of MA, catechol moieties and Fe^{3+} ions. For the *in vitro* test, NIH 3T3 fibroblasts were encapsulated within the hydrogel, and photocrosslinked using visible light. The 3D cultures were incubated at 37 °C in a 5% CO_2 humidified atmosphere for 7 days, and the growth medium was replaced every 2 days. Fig. 4 showed cell viability and metabolic activity of 3D encapsulated NIH 3T3 fibroblast cells inside GelMAC-Fe and GelMA-Fe hydrogels. Live/dead images of the 3D

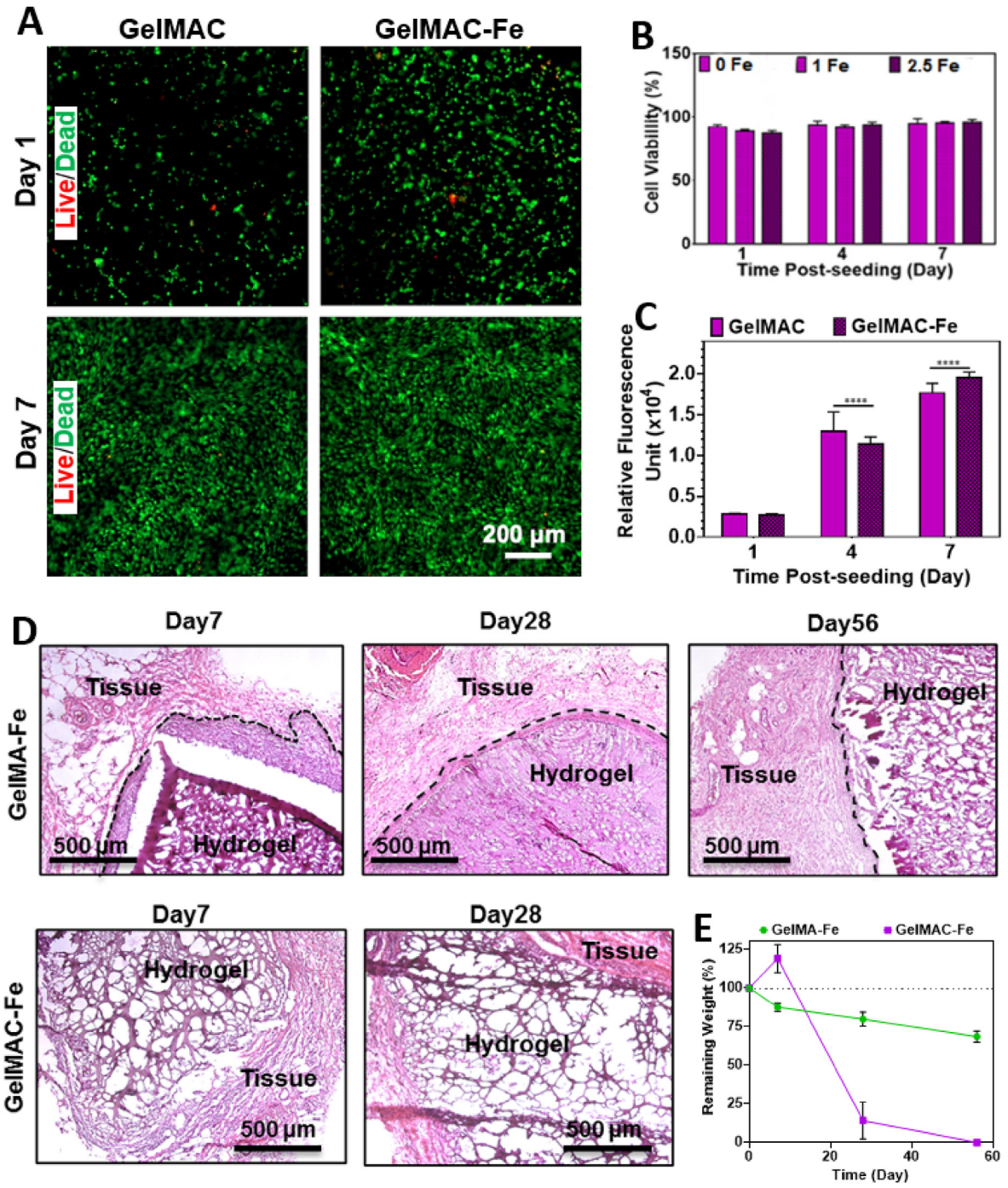

Fig. 4. *In vitro* and *in vivo* biocompatibility of GelMA and GelMAC hydrogels after subcutaneous implantation. A) Representative live/dead images of 3D encapsulated fibroblasts in GelMAC and GelMAC-Fe hydrogels, and **B)** Cell viability of 3D-encapsulated NIH 3T3 fibroblast cells in GelMAC hydrogels containing 0, 1, and 2.5 mM Fe^{3+} ion concentration on day 1, 4, and 7 post-encapsulation, **C)** Metabolic activity of fibroblasts measured by PrestoBlue™ cell viability reagents on 1, 4, and 7 days post-incubation. **D)** H&E-stained sections of subcutaneously implanted hydrogels after 7, 28, and 56 days of implantation. **E)** *In vivo* biodegradation of hydrogels on days 7, 28, and 56 post-implantation (n = 4). Data are represented as mean ± SD (*p < 0.05, **p < 0.01, and ****p < 0.0001, n ≥ 6).

encapsulated fibroblasts in GelMAC-Fe and GelMAC-Fe hydrogels are presented in Fig. 4A. Cell-laden GelMAC-Fe hydrogels were predominantly comprised of viable and proliferating fibroblast cells over the 7 days post-encapsulation. Cell viability inside GelMAC hydrogels incorporating different Fe^{3+} ion concentrations were found to be >95% over 7 days of post-encapsulation (Fig. 4B). The metabolic activity of 3T3 fibroblasts was also measured on 1, 4, and 7 days post-incubations (Fig. 4C) which were observed to consistently increase until day 7. These results demonstrated that the GelMAC-Fe hydrogel could support the viability, proliferation, and spreading of NIH 3T3 fibroblast cells *in vitro*. This also suggests that GelMAC-Fe hydrogels can be potentially used as a platform for cell delivery for different kinds of wounds [77].

In vivo biocompatibility and biodegradation of GelMA-Fe and GelMAC-Fe hydrogels were also assessed by using a rat subcutaneous implantation model. Here, hydrogels were implanted in subcutaneous pockets, prepared along the dorsomedial skin of male Wistar rats and examined after 7, 28 and 56 days post-implantation. Fig. 4D presents the H&E-stained histological images of retrieved hydrogels at different days post-surgery. Interestingly, cells were observed to make their way inside the GelMAC-Fe hydrogel easier than GelMA-Fe due to the loser hydrogel network of GelMAC-Fe. This was observed by higher cell infiltration inside GelMAC-Fe hydrogel while a dense layer of cells (indicated by black dashed lines) was observed around GelMA-Fe at day 7 after surgery. This is in accordance with previous studies that points out to the infiltration of different kind of cells (i.e., leukocytes, macrophages, fibroblasts) to the hydrogel implantation site [78–80]. On the other hand, thickness of the dense cell layer (indicated by black dashed lines) around GelMA-Fe implants decreased significantly by day 28 (Fig. 4D). Hereafter, the *in vivo* biodegradation of the hydrogels was evaluated by measuring the changes in the weight (percentage value) of the explanted samples at 7, 28, and 56 days post-implantation (Fig. 4E). For the GelMAC-Fe sealant, weight of the explanted hydrogel was observed to increase slightly at day 7 followed by a significant decrease at day 28 and complete elimination at day 56. Such increase in the weight of the hydrogel could be related to the cell infiltration inside the hydrogels and the deposition of extracellular matrix (ECM) components while hydrogel network is almost intact (Fig. 4D). Meanwhile, GelMAC-Fe also enabled cellular ingrowth and facilitated the complete replacement of the hydrogel with autologous tissue 28 days post-implantation (Fig. 4D). This finding is most likely associated with the catechol mediated production of reactive oxygen species (ROS) which accelerate the immune cell metabolism (e.g., T Cells, Macrophages) [81–83]. Moreover, natural healing response starts with inflammatory cell infiltration stages [84]. Therefore, catechol groups in GelMAC-Fe improved tissue adhesiveness of hydrogel and can facilitate tissue healing, which causes the faster resorption of the implanted hydrogel as compared to GelMA-Fe.

3.5. *In vivo* hemostatic efficacy of GelMAC hemostatic sealant

In vivo hemostatic efficacy of the GelMAC hydrogel was tested and analyzed using a rat liver bleeding model. Six experimental groups were tested, which included four groups of bioadhesives (GelMA, GelMAC, GelMA-Fe, and GelMAC-Fe), and two control groups (injury only as negative control and commercially available Surgicel® as the positive control), and four animals per experimental group were tested. Immediately after creating a standardized liver wound using a 2 mm-biopsy punch, hemostatic bioadhesives were applied to the bleeding lesion and crosslinked for 4 min using a visible light source (Fig. 5A–E). Any blood loss from the incision site (from the time of incision to complete coagulation) was collected on a filter paper for the duration of 4 min and weighted immediately afterward. Although after applying the prepolymer solution, visible light was irradiated for 4 min to achieve maximum crosslinking and improved mechanical properties, the prepolymer solution could immediately interact with the blood, adhere to the wound surface, initiate clotting on the injury site, and stop bleeding after around 40 s (Video S1). This was shown in Fig. 5C, where application of GelMAC

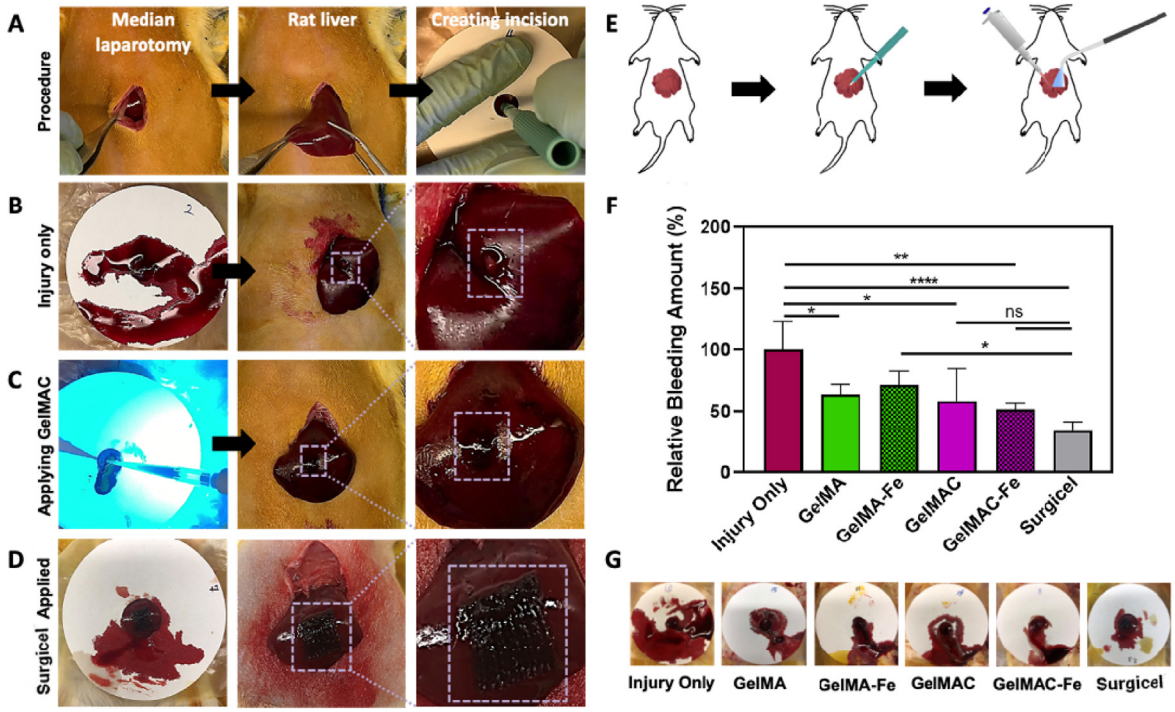

Fig. 5. *In vivo* hemostatic efficacy of the GelMA and GelMAC hydrogels in a rat liver bleeding model. **A)** Images of the surgical procedure. **B)** Liver wound site post-puncture and without any treatment. **C)** Application and photocrosslinking of the GelMAC hydrogels at the wound site. **D)** Application of the commercial hemostatic agent Surgicel®. **E)** A schematic depicting the application and photocrosslinking of the GelMA and GelMAC hydrogels. **F)** Relative bleeding amount for each study group in comparison to the blood mass collected on the filter paper for the injury only group. **G)** Representative images of the blood collected on the filter papers for each experimental group. Data are represented as mean ± SD (*$p < 0.05$, **$p < 0.01$, and ****$p < 0.0001$, $n = 4$).

prepolymer solution and *in situ* photocrosslinking stopped bleeding immediately with minimal wetting of the filter paper. Meanwhile, GelMAC-Fe and GelMA-Fe groups demonstrated 48.1 ± 4.9% and 28.6 ± 11.4% reduction in bleeding, respectively (Fig. 5F). The percentage of reduction in bleeding for GelMAC and GelMA hydrogels were 41.8 ± 26.6% and 36.2 ± 8.3%, respectively (Fig. 5F). Interestingly, GelMAC and GelMAC-Fe groups showed comparable reduction in bleeding with Surgicel® (positive control), 66.3 ± 7.6%. However, Surgicel® lacks adhesive characteristics in the injury site. On the other hand, GelMAC-Fe hemostatic sealant along with its excellent hemostatic efficacy (comparable to Surgicel®), it also adhered to the tissue site and stayed intact after 1-week post-operation.

Supplementary data related to this article can be found at https://doi.org/10.1016/j.mtbio.2021.100199.

Representative images of the collected blood mass on the filter paper are shown for each experimental group in Fig. 5G. These representative images allowed us to further qualitatively analyze the mass of the blood collected post-treatment, which was in agreement with our quantitative measurements and analysis. All the hydrogel-treated experimental groups were effectively covered and remained adhered to the original incision sites, with no abdominal organ adhesion or prominent discoloration observed. The utility of low concentration of Fe^{3+} ions in the formation of GelMA-Fe and GelMAC-Fe hydrogels did not demonstrate any toxicity *in vivo*, which is in agreement with the *in vitro* and *in vivo* cytotoxicity results obtained (Fig. 5A and B). Overall, our results confirmed the excellent hemostatic activity of GelMAC-Fe hydrogels through the synergistic effect of catechol groups and ferric ions.

4. Conclusions

In this work, we have engineered a new multifunctional hemostatic sealant, named as GelMAC, for the sealing of internal soft tissues. Double-crosslinked GelMAC hydrogels were synthesized based on chemically modified gelatin molecules which contained covalently conjugated catechol motifs and MA functionalities. While incorporation of Fe^{3+} ion enhanced the mechanical properties of the resulting hydrogel, catechol moieties facilitated the wet tissue adhesion. Adhesion strength of GelMAC hydrogel was comparable with the commercial surgical sealants and superior with respect to the commercial hemostatic sealant. Cytocompatibility of GelMAC hydrogel was confirmed *in vitro* and *in vivo* using fibroblast cells and a rat subcutaneous model. Finally, hemostatic capability of the GelMAC hydrogel was demonstrated and compared with Surgicel®, a widely used clinical hemostat with no tissue adhesive property. *In vitro* blood clotting assay showed a significantly decreased clotting time for GelMAC compared to Surgical. During *in vivo* liver bleeding test in rats, GelMAC hydrogel was observed to close the incision rapidly and stop bleeding. This performance was comparable with Surgicel®, while adhesive characteristics of the GelMAC was unaltered. Therefore, GelMAC based hemostatic sealant can potentially be used to control hemorrhage in soft and dynamic internal organs where the use of sutures, staples, or wires is limited.

Future work will focus on evaluating the ability of this system to reduce the risk of infection after traumatic injury as well as incorporating a more physiologically relevant animal model for surgical wounds. This is mainly because wounds are highly susceptible to microbial infection and biofilm formation, especially in patients with impaired and dysfunctional immune system.

Credit author statement

Sevana Baghdasarian- Conceptualization, Methodology, Validation, Formal analysis, Investigation, Writing – original draft, Writing – review & editing, Visualization, Bahram Saleh- Conceptualization, Methodology, Validation, Formal analysis, Investigation, Writing – original draft, Writing – review & editing, Visualization, Avijit Baidya- Investigation, Formal analysis, Methodology, Writing – original draft, Writing – review & editing, Hanjun Kim- Investigation, Formal analysis, Methodology, Mahsa Ghovvati- Investigation, Formal analysis, Methodology, Writing – original draft, Writing – review & editing, Ehsan Shirzaei Sani- Investigation, Formal analysis, Reihaneh Haghniaz- Investigation, Formal analysis, Methodology, Shashank Madhu- Investigation, Formal analysis, Maria Kanelli- Investigation, Formal analysis, Iman Noshadi- Conceptualization, Methodology, Writing – review & editing, Nasim Annabi- Conceptualization, Methodology, Validation, Supervision, Project administration, Funding acquisition, Recourses, Writing – original draft, Writing – review & editing.

Declaration of competing interest

The authors declare the following financial interests/personal relationships which may be considered as potential competing interests: N. A. hold equity in GelMEDIX Inc.

Acknowledgements

N.A. acknowledges the support from the National Institutes of Health (R01-EB023052; R01HL140618). The authors acknowledge Professor Reza Abdi for his help in analyzing the *in vivo* data and Professor Art Coury for his help in synthesizing the biomaterials.

Appendix A. Supplementary data

Supplementary data to this article can be found online at https://doi:10.1016/j.mtbio.2021.100199.

References

[1] S.I. Berríos-Torres, C.A. Umscheid, D.W. Bratzler, B. Leas, E.C. Stone, R.R. Kelz, C.E. Reinke, S. Morgan, J.S. Solomkin, J.E. Mazuski, E.P. Dellinger, K.M.F. Itani, E.F. Berbari, J. Segreti, J. Parvizi, J. Blanchard, G. Allen, J.A.J.W. Kluytmans, R. Donlan, W.P. Schecter, F.T.H.I.C.P.A. Committee, Centers for disease control and prevention guideline for the prevention of surgical site infection, JAMA Surgery 152 (8) (2017) 784–791, 2017.

[2] I. Galanakis, N. Vasdev, N. Soomro, A review of current hemostatic agents and tissue sealants used in laparoscopic partial nephrectomy, Rev. Urol. 13 (3) (2011) 131–138.

[3] W.D. Spotnitz, S. Burks, Hemostats, sealants, and adhesives: components of the surgical toolbox, Transfusion 48 (7) (2008) 1502–1516.

[4] O. Chiara, S. Cimbanassi, G. Bellanova, M. Chiarugi, A. Mingoli, G. Olivero, S. Ribaldi, G. Tugnoli, S. Basilicò, F. Bindi, L. Briani, F. Renzi, P. Chirletti, G. Di Grezia, A. Martino, R. Marzaioli, G. Noschese, N. Portolani, P. Ruscelli, M. Zago, S. Sgardello, F. Stagnitti, S. Miniello, A systematic review on the use of topical hemostats in trauma and emergency surgery, BMC Surg. 18 (1) (2018) 68.

[5] D.H. Sierra, Fibrin sealant adhesive systems: a review of their chemistry, material properties and clinical applications, J. Biomater. Appl. 7 (4) (1993) 309–352.

[6] M.R. Jackson, Fibrin sealants in surgical practice: an overview, Am. J. Surg. 182 (2 Suppl) (2001) 1s–7s.

[7] S.H. Baik, J.H. Kim, H.H. Cho, S.N. Park, Y.S. Kim, H. Suh, Development and analysis of a collagen-based hemostatic adhesive, J. Surg. Res. 164 (2) (2010) e221–e228.

[8] I. Grabska-Liberek, R. Galus, W. Owczarek, K. Włodarsk, S. Zabielski, J. Malejczyk, D. Sladowski, [Collagen based dressings in the treatment of wound healing], Pol. Merkur. Lek. 35 (205) (2013) 51–54.

[9] C.M. Elvin, T. Vuocolo, A.G. Brownlee, L. Sando, M.G. Huson, N.E. Liyou, P.R. Stockwell, R.E. Lyons, M. Kim, G.A. Edwards, G. Johnson, G.A. McFarland, J.A. Ramshaw, J.A. Werkmeister, A highly elastic tissue sealant based on photopolymerised gelatin, Biomaterials 31 (32) (2010) 8323–8331.

[10] M. Tavafoghi, A. Sheikhi, R. Tutar, J. Jahangiry, A. Baidya, R. Haghniaz, A. Khademhosseini, Engineering tough, injectable, naturally derived, bioadhesive composite hydrogels, Adv. Healthcare Mater. 9 (10) (2020), 1901722.

[11] M.A. Brown, M.R. Daya, J.A. Worley, Experience with chitosan dressings in a civilian EMS system, J. Emerg. Med. 37 (1) (2009) 1–7.

[12] P.R. Klokkevold, H. Fukayama, E.C. Sung, C.N. Bertolami, The effect of chitosan (poly-N-acetyl glucosamine) on lingual hemostasis in heparinized rabbits, J. Oral Maxillofac. Surg. 57 (1) (1999) 49–52.

[13] J. Quinn, G. Wells, T. Sutcliffe, M. Jarmuske, J. Maw, I. Stiell, P. Johns, A randomized trial comparing octylcyanoacrylate tissue adhesive and sutures in the management of lacerations, JAMA 277 (19) (1997) 1527–1530.

[14] T.B. Reece, T.S. Maxey, I.L. Kron, A prospectus on tissue adhesives, Am. J. Surg. 182 (2 Suppl) (2001) 40s–44s.

[15] A.P. Duarte, J.F. Coelho, J.C. Bordado, M.T. Cidade, M.H. Gil, Surgical adhesives: systematic review of the main types and development forecast, Prog. Polym. Sci. 37 (8) (2012) 1031–1050.

[16] A.J. Singer, H.C. Thode Jr., A review of the literature on octylcyanoacrylate tissue adhesive, Am. J. Surg. 187 (2) (2004) 238–248.
[17] M.B. Edmonson, Foreign body reactions to dermabond, Am. J. Emerg. Med. 19 (3) (2001) 240–241.
[18] N. Annabi, D. Rana, E. Shirzaei Sani, R. Portillo-Lara, J.L. Gifford, M.M. Fares, S.M. Mithieux, A.S. Weiss, Engineering a sprayable and elastic hydrogel adhesive with antimicrobial properties for wound healing, Biomaterials 139 (2017) 229–243.
[19] H. Lee, B.P. Lee, P.B. Messersmith, A reversible wet/dry adhesive inspired by mussels and geckos, Nature 448 (7151) (2007) 338–341.
[20] N. Lang, M.J. Pereira, Y. Lee, I. Friehs, N.V. Vasilyev, E.N. Feins, K. Ablasser, E.D. O'Cearbhaill, C. Xu, A. Fabozzo, R. Padera, S. Wasserman, F. Freudenthal, L.S. Ferreira, R. Langer, J.M. Karp, P.J. del Nido, A blood-resistant surgical glue for minimally invasive repair of vessels and heart defects, Sci. Transl. Med. 6 (218) (2014), 218ra6.
[21] L. Han, L. Yan, K. Wang, L. Fang, H. Zhang, Y. Tang, Y. Ding, L.-T. Weng, J. Xu, J. Weng, Y. Liu, F. Ren, X. Lu, Tough, self-healable and tissue-adhesive hydrogel with tunable multifunctionality, NPG Asia Mater. 9 (4) (2017) e372, e372.
[22] C. Fuller, Reduction of intraoperative air leaks with Progel in pulmonary resection: a comprehensive review, J. Cardiothorac. Surg. 8 (1) (2013) 90.
[23] P. Kord Forooshani, B.P. Lee, Recent approaches in designing bioadhesive materials inspired by mussel adhesive protein, J. Polym. Sci. Polym. Chem. 55 (1) (2017) 9–33.
[24] H. Lee, N.F. Scherer, P.B. Messersmith, Single-molecule mechanics of mussel adhesion, Proc. Natl. Acad. Sci. Unit. States Am. 103 (35) (2006) 12999–13003.
[25] M. Yu, J. Hwang, T.J. Deming, Role of l-3,4-Dihydroxyphenylalanine in mussel adhesive proteins, J. Am. Chem. Soc. 121 (24) (1999) 5825–5826.
[26] L. Han, Y. Zhang, X. Lu, K. Wang, Z. Wang, H. Zhang, Polydopamine nanoparticles modulating stimuli-responsive PNIPAM hydrogels with cell/tissue adhesiveness, ACS Appl. Mater. Interfaces 8 (42) (2016) 29088–29100.
[27] H. Lee, J. Rho, P.B. Messersmith, Facile conjugation of biomolecules onto surfaces via mussel adhesive protein inspired coatings, Adv. Mater. 21 (4) (2009) 431–434.
[28] H. Zhang, L.P. Bré, T. Zhao, Y. Zheng, B. Newland, W. Wang, Mussel-inspired hyperbranched poly(amino ester) polymer as strong wet tissue adhesive, Biomaterials 35 (2) (2014) 711–719.
[29] J. Yang, R. Bai, B. Chen, Z. Suo, Hydrogel adhesion: a supramolecular synergy of chemistry, topology, and mechanics, Adv. Funct. Mater. 30 (2) (2020), 1901693.
[30] J.Y. Kim, S.B. Ryu, K.D. Park, Preparation and characterization of dual-crosslinked gelatin hydrogel via Dopa-Fe3+ complexation and fenton reaction, J. Ind. Eng. Chem. 58 (2018) 105–112.
[31] W. Zhang, R. Wang, Z. Sun, X. Zhu, Q. Zhao, T. Zhang, A. Cholewinski, F. Yang, B. Zhao, R. Pinnaratip, P.K. Forooshani, B.P. Lee, Catechol-functionalized hydrogels: biomimetic design, adhesion mechanism, and biomedical applications, Chem. Soc. Rev. 49 (2) (2020) 433–464.
[32] W.-Y. Quan, Z. Hu, H.-Z. Liu, Q.-Q. Ouyang, D.-Y. Zhang, S.-D. Li, P.-W. Li, Z.-M. Yang, Mussel-inspired catechol-functionalized hydrogels and their medical applications, Molecules 24 (14) (2019), 2586.
[33] S. Pourshahrestani, E. Zeimaran, N.A. Kadri, N. Mutlu, A.R. Boccaccini, Polymeric hydrogel systems as emerging biomaterial platforms to enable hemostasis and wound healing, Adv. Healthcare Mater. 9 (20) (2020), 2000905.
[34] A.M. Behrens, M.J. Sikorski, P. Kofinas, Hemostatic strategies for traumatic and surgical bleeding, J. Biomed. Mater. Res. 102 (11) (2014) 4182–4194.
[35] Y. Hong, F. Zhou, Y. Hua, X. Zhang, C. Ni, D. Pan, Y. Zhang, D. Jiang, L. Yang, Q. Lin, Y. Zou, D. Yu, D.E. Arnot, X. Zou, L. Zhu, S. Zhang, H. Ouyang, A strongly adhesive hemostatic hydrogel for the repair of arterial and heart bleeds, Nat. Commun. 10 (1) (2019), 2060.
[36] T.A. Ostomel, Q. Shi, P.K. Stoimenov, G.D. Stucky, Metal oxide surface charge mediated hemostasis, Langmuir 23 (22) (2007) 11233–11238.
[37] B. Bordes, D. Martin, B. Schloss, A. Beebe, W. Samora, J. Klamar, D. Stukus, J.D. Tobias, Intraoperative anaphylactic reaction: is it the Floseal? J. Pediatr. Pharmacol. Therapeut. 21 (4) (2016) 358–365.
[38] C. Li, C. Mu, W. Lin, T. Ngai, Gelatin effects on the physicochemical and hemocompatible properties of gelatin/PAAm/laponite nanocomposite hydrogels, ACS Appl. Mater. Interfaces 7 (33) (2015) 18732–18741.
[39] G. Lokhande, J.K. Carrow, T. Thakur, J.R. Xavier, M. Parani, K.J. Bayless, A.K. Gaharwar, Nanoengineered injectable hydrogels for wound healing application, Acta Biomater. 70 (2018) 35–47.
[40] N. Golafshan, R. Rezahasani, M. Tarkesh Esfahani, M. Kharaziha, S.N. Khorasani, Nanohybrid hydrogels of laponite: PVA-Alginate as a potential wound healing material, Carbohydr. Polym. 176 (2017) 392–401.
[41] A.K. Gaharwar, R.K. Avery, A. Assmann, A. Paul, G.H. McKinley, A. Khademhosseini, B.D. Olsen, Shear-thinning nanocomposite hydrogels for the treatment of hemorrhage, ACS Nano 8 (10) (2014) 9833–9842.
[42] L. Wang, X. Zhang, K. Yang, Y.V. Fu, T. Xu, S. Li, D. Zhang, L.N. Wang, C.S. Lee, A novel double-crosslinking-double-network design for injectable hydrogels with enhanced tissue adhesion and antibacterial capability for wound treatment, Adv. Funct. Mater. 30 (1) (2020), 1904156.
[43] J. Jennings, Controlling chitosan degradation properties in vitro and in vivo, Chitosan Based Biomater. 1 (2017) 159–182. Elsevier.
[44] S. Keshavarzi, M. MacDougall, D. Lulic, A. Kasasbeh, M. Levy, Clinical experience with the surgicel family of absorbable hemostats (oxidized regenerated cellulose) in neurosurgical applications: a review, Wounds 25 (6) (2013) 160–167.
[45] K. Yue, X. Li, K. Schrobback, A. Sheikhi, N. Annabi, J. Leijten, W. Zhang, Y.S. Zhang, D.W. Hutmacher, T.J. Klein, A. Khademhosseini, Structural analysis of photocrosslinkable methacryloyl-modified protein derivatives, Biomaterials 139 (2017) 163–171.
[46] X. Zhou, Z. Luo, A. Baidya, H.-j. Kim, C. Wang, X. Jiang, M. Qu, J. Zhu, L. Ren, F. Vajhadin, P. Tebon, N. Zhang, Y. Xue, Y. Feng, C. Xue, Y. Chen, K. Lee, J. Lee, S. Zhang, C. Xu, N. Ashammakhi, S. Ahadian, M.R. Dokmeci, Z. Gu, W. Sun, A. Khademhosseini, Biodegradable β-cyclodextrin conjugated gelatin methacryloyl microneedle for delivery of water-insoluble drug, Adv. Healthcare Mater. 9 (11) (2020), 2000527.
[47] N. Kaneko, M. Ghovvati, Y. Komuro, L. Guo, K. Khatibi, L.L. Ponce Mejia, H. Saber, N. Annabi, S. Tateshima, A new aspiration device equipped with a hydro-separator for acute ischemic stroke due to challenging soft and stiff clots, Intervent Neuroradiol. (2021), 15910199211015060.
[48] M.F. Shih, M.D. Shau, M.Y. Chang, S.K. Chiou, J.K. Chang, J.Y. Cherng, Platelet adsorption and hemolytic properties of liquid crystal/composite polymers, Int. J. Pharm. 327 (1–2) (2006) 117–125.
[49] A.H.J. Gowda, Y. Bu, O. Kudina, K.V. Krishna, R.A. Bohara, D. Eglin, A. Pandit, Design of tunable gelatin-dopamine based bioadhesives, Int. J. Biol. Macromol. 164 (2020) 1384–1391.
[50] I. Noshadi, S. Hong, K.E. Sullivan, E. Shirzaei Sani, R. Portillo-Lara, A. Tamayol, S.R. Shin, A.E. Gao, W.L. Stoppel, L.D. Black Iii, A. Khademhosseini, N. Annabi, In vitro and in vivo analysis of visible light crosslinkable gelatin methacryloyl (GelMA) hydrogels, Biomater. Sci. 5 (10) (2017) 2093–2105.
[51] W.Y. Quan, Z. Hu, H.Z. Liu, Q.Q. Ouyang, D.Y. Zhang, S.D. Li, P.W. Li, Z.M. Yang, Mussel-inspired catechol-functionalized hydrogels and their medical applications, Molecules 24 (14) (2019).
[52] J. Guo, W. Sun, J.P. Kim, X. Lu, Q. Li, M. Lin, O. Mrowczynski, E.B. Rizk, J. Cheng, G. Qian, J. Yang, Development of tannin-inspired antimicrobial bioadhesives, Acta Biomater. 72 (2018) 35–44.
[53] T. Yadav, V. Mukherjee, Interpretation of IR and Raman spectra of dopamine neurotransmitter and effect of hydrogen bond in HCl, J. Mol. Struct. 1160 (2018) 256–270.
[54] C.D. Spicer, E.T. Pashuck, M.M. Stevens, Achieving controlled biomolecule–biomaterial conjugation, Chem. Rev. 118 (16) (2018) 7702–7743.
[55] F. Zha, Z. Yang, J. Rao, B. Chen, Conjugation of pea protein isolate via maillard-driven chemistry with saccharide of diverse molecular mass: molecular interactions leading to aggregation or glycation, J. Agric. Food Chem. 68 (37) (2020) 10157–10166.
[56] J. Rickman, G. Tronci, H. Liang, S.J. Russell, Rotation-assisted wet-spinning of UV-cured gelatin fibres and nonwovens, J. Mater. Sci. 54 (14) (2019) 10529–10547.
[57] C. Cao, E. Kim, Y. Liu, M. Kang, J. Li, J.J. Yin, H. Liu, X. Qu, C. Liu, W.E. Bentley, G.F. Payne, Radical scavenging activities of biomimetic catechol-chitosan films, Biomacromolecules 19 (8) (2018) 3502–3514.
[58] J. Hu, L. Yang, P. Yang, S. Jiang, X. Liu, Y. Li, Polydopamine free radical scavengers, Biomater. Sci. 8 (18) (2020) 4940–4950.
[59] N. Asadi, H. Pazoki-Toroudi, A.R. Del Bakhshayesh, A. Akbarzadeh, S. Davaran, N. Annabi, Multifunctional hydrogels for wound healing: special focus on biomacromolecular based hydrogels, Int. J. Biol. Macromol. 170 (2021) 728–750.
[60] H. Montazerian, A. Baidya, R. Haghniaz, E. Davoodi, S. Ahadian, N. Annabi, A. Khademhosseini, P.S. Weiss, Stretchable and bioadhesive gelatin methacryloyl-based hydrogels enabled by in situ dopamine polymerization, ACS Appl. Mater. Interfaces 13 (34) (2021) 40290–40301.
[61] S. Hong, D. Pirovich, A. Kilcoyne, C.H. Huang, H. Lee, R. Weissleder, Supramolecular metallo-bioadhesive for minimally invasive use, Adv. Mater. 28 (39) (2016) 8675–8680.
[62] P.S. Yavvari, S. Pal, S. Kumar, A. Kar, A.K. Awasthi, A. Naaz, A. Srivastava, A. Bajaj, Injectable, self-healing chimeric catechol-Fe(III) hydrogel for localized combination cancer therapy, ACS Biomater. Sci. Eng. 3 (12) (2017) 3404–3413.
[63] M. Rahimnejad, W. Zhong, Mussel-inspired hydrogel tissue adhesives for wound closure, RSC Adv. 7 (75) (2017) 47380–47396.
[64] W.-C. Huang, F. Ali, J. Zhao, K. Rhee, C. Mou, C.J. Bettinger, Ultrasound-mediated self-healing hydrogels based on tunable metal–organic bonding, Biomacromolecules 18 (4) (2017) 1162–1171.
[65] C. Gong, C. Lu, B. Li, M. Shan, G. Wu, Injectable dopamine-modified poly(α,β-aspartic acid) nanocomposite hydrogel as bioadhesive drug delivery system, J. Biomed. Mater. Res. 105 (4) (2017) 1000–1008.
[66] H. Cheng, K. Yue, M. Kazemzadeh-Narbat, Y. Liu, A. Khalilpour, B. Li, Y.S. Zhang, N. Annabi, A. Khademhosseini, Mussel-inspired multifunctional hydrogel coating for prevention of infections and enhanced osteogenesis, ACS Appl. Mater. Interfaces 9 (13) (2017) 11428–11439.
[67] Y.-F. Zhao, J.-Y. Zhao, W.-Z. Hu, K. Ma, Y. Chao, P.-J. Sun, X.-B. Fu, H. Zhang, Synthetic poly(vinyl alcohol)–chitosan as a new type of highly efficient hemostatic sponge with blood-triggered swelling and high biocompatibility, J. Mater. Chem. B 7 (11) (2019) 1855–1866.
[68] M.H. MacDonald, A.Y. Wang, J.W. Clymer, R.W. Hutchinson, R. Kocharian, An in vivo comparison of the efficacy of hemostatic powders, using two porcine bleeding models, Med. Dev. (Auckl) 10 (2017) 273–279.
[69] Y. Zhong, X. Zhao, G. Li, D. Zhang, D. Wang, Mussel-inspired hydrogels as tissue adhesives for hemostasis with fast-forming and self-healing properties, Eur. Polym. J. 148 (2021), 110361.
[70] M. Mehdizadeh, J. Yang, Design strategies and applications of tissue bioadhesives, Macromol. Biosci. 13 (3) (2013) 271–288.
[71] M. Shin, J.H. Ryu, K. Kim, M.J. Kim, S. Jo, M.S. Lee, D.Y. Lee, H. Lee, Hemostatic swabs containing polydopamine-like catecholamine chitosan-catechol for normal and coagulopathic animal models, ACS Biomater. Sci. Eng. 4 (7) (2018) 2314–2318.
[72] M. Shin, S.G. Park, B.C. Oh, K. Kim, S. Jo, M.S. Lee, S.S. Oh, S.H. Hong, E.C. Shin, K.S. Kim, S.W. Kang, H. Lee, Complete prevention of blood loss with self-sealing haemostatic needles, Nat. Mater. 16 (1) (2017) 147–152.

[73] Y.X. Zhao, B.Y. Gao, H.K. Shon, B.C. Cao, J.H. Kim, Coagulation characteristics of titanium (Ti) salt coagulant compared with aluminum (Al) and iron (Fe) salts, J. Hazard. Mater. 185 (2–3) (2011) 1536–1542.
[74] B. Guo, R. Dong, Y. Liang, M. Li, Haemostatic materials for wound healing applications, Nat. Rev. Chem. 5 (11) (2021) 773–791.
[75] M.B. Ashour, S.J. Gee, B.D. Hammock, Use of a 96-well microplate reader for measuring routine enzyme activities, Anal. Biochem. 166 (2) (1987) 353–360.
[76] C. Zhou, Z. Yi, Blood-compatibility of polyurethane/liquid crystal composite membranes, Biomaterials 20 (22) (1999) 2093–2099.
[77] Q. Xu, A. Sigen, Y. Gao, L. Guo, J. Creagh-Flynn, D. Zhou, U. Greiser, Y. Dong, F. Wang, H.J.A.b. Tai, A hybrid injectable hydrogel from hyperbranched PEG macromer as a stem cell delivery and retention platform for diabetic wound, Healing 75 (2018) 63–74.
[78] H. Meng, Y. Liu, B.P. Lee, Model polymer system for investigating the generation of hydrogen peroxide and its biological responses during the crosslinking of mussel adhesive moiety, Acta Biomater. 48 (2017) 144–156.
[79] H. Meng, Y. Li, M. Faust, S. Konst, B.P. Lee, Hydrogen peroxide generation and biocompatibility of hydrogel-bound mussel adhesive moiety, Acta Biomater. 17 (2015) 160–169.
[80] A. Assmann, A. Vegh, M. Ghasemi-Rad, S. Bagherifard, G. Cheng, E.S. Sani, G.U. Ruiz-Esparza, I. Noshadi, A.D. Lassaletta, S. Gangadharan, A. Tamayol, A. Khademhosseini, N. Annabi, A highly adhesive and naturally derived sealant, Biomaterials 140 (2017) 115–127.
[81] D.M. Previte, E.C. O'Connor, E.A. Novak, C.P. Martins, K.P. Mollen, J.D. Piganelli, Reactive oxygen species are required for driving efficient and sustained aerobic glycolysis during CD4+ T cell activation, PLoS One 12 (4) (2017), e0175549.
[82] H.S. Shin, H. Satsu, M.J. Bae, M. Totsuka, M. Shimizu, Catechol groups enable reactive oxygen species scavenging-mediated suppression of PKD-NFkappaB-IL-8 signaling pathway by chlorogenic and caffeic acids in human intestinal cells, Nutrients 9 (2) (2017).
[83] D.G. Franchina, C. Dostert, D. Brenner, Reactive oxygen species: involvement in T cell signaling and metabolism, Trends Immunol. 39 (6) (2018) 489–502.
[84] C.A. Oskeritzian, Mast cells and wound healing, Adv. Wound Care 1 (1) (2012) 23–28.